

## Supplementary Information

# Solvent Dependent Triplet State Delocalization in a Co-facial Porphyrin Heterodimer

Susanna Ciuti<sup>a</sup>, Jacopo Toninato<sup>a</sup>, Antonio Barbon<sup>a</sup>, Niloofar Zarrabi<sup>b</sup>, Prashanth K. Poddutoori<sup>\*b</sup>,  
Art van der Est<sup>\*c</sup>, Marilena Di Valentin<sup>\*a</sup>

<sup>a</sup>Dipartimento di Scienze Chimiche, Università degli studi di Padova, Via Marzolo 1, 35131 Padova, Italy.

<sup>b</sup>Department of Chemistry & Biochemistry, University of Minnesota Duluth, 1039 45 University Drive, Duluth, Minnesota 55812, USA.

<sup>c</sup>Department of Chemistry, Brock University, 1812 Sir Isaac Brock Way, St. Catharines, Ontario, L2S 3A1, Canada.

## 1. Calculated UV/Vis Absorption Wavelengths and Transition Dipole Moments

Fig. S1 shows the  $Q_x$  and  $Q_y$  transition dipole moments of the two monomers AlPor-OH and PPor-OMe-PF<sub>6</sub> obtained from quantum chemical computations. The computed and experimental wavelengths and oscillator strengths of the transitions are given in Tables S1 and S2.

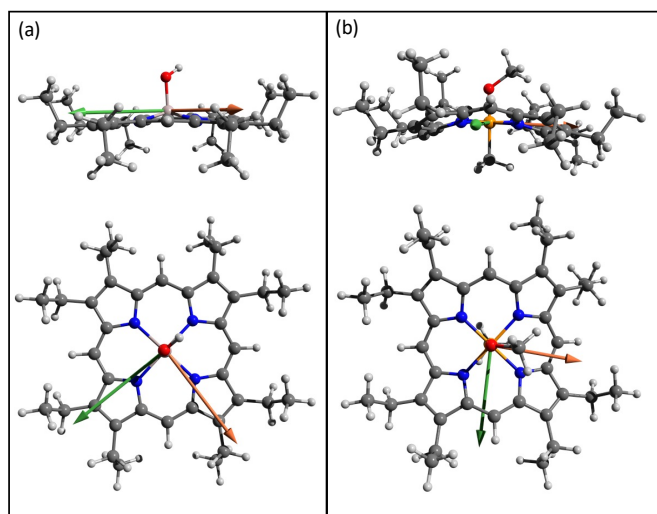


**Fig. S1.** Transition dipole moments of the lowest energy excitations of the porphyrin monomers obtained from CASSCF-NEVPT2 calculations. (a) AlPorOH (b) PPor-OMe\*. The  $Q_x$  transition dipole is shown in green, the  $Q_y$  dipole is shown in orange.

**Table S1** Computed and experimental absorption wavelengths and oscillator strengths for AlPor-OH

Method	$Q_x$		$Q_y$	
	$\lambda$ (nm)	$f_{osc}$	$\lambda$ (nm)	$f_{osc}$
TDDFT PBE	549.7	0.0052	548.5	0.0056
TDDFT CAM-B3LYP	503.1	0.029	502.2	0.023
CASSCF	412.6	0.063	409.7	0.063
CASSCF-NEVPT2	587.6	0.044	584.6	0.044
Experiment	569	0.042		

Method	$B_x$		$B_y$	
	$\lambda$ (nm)	$f_{osc}$	$\lambda$ (nm)	$f_{osc}$
TDDFT PBE	420.7	0.021	417.9	0.026
TDDFT CAM-B3LYP	306.1	0.97	305.1	1.03
CASSCF	249.8	2.50	249.5	2.52
CASSCF-NEVPT2	403.2	1.55	403.0	1.54
Experiment	397	0.92		

**Table S2** Computed and experimental absorption wavelengths and oscillator strengths for PPor-OMe-PF<sub>6</sub>

Method	$Q_x$		$Q_y$	
	$\lambda$ (nm)	$f_{osc}$	$\lambda$ (nm)	$f_{osc}$
TDDFT PBE	562.3	0.0014	559.9	0.0022
TDDFT CAM-B3LYP	517.0	0.013	515.3	0.011
CASSCF	418.4	0.039	413.7	0.047
CASSCF-NEVPT2	606.5	0.032	606.2	0.027
Experiment	591	0.033		

Method	$B_x$		$B_y$	
	$\lambda$ (nm)	$f_{osc}$	$\lambda$ (nm)	$f_{osc}$
TDDFT PBE	435.1	0.0027	433.0	0.0038
TDDFT CAM-B3LYP	314.8	0.79	313.9	0.71
CASSCF	253.7	2.17	252.9	2.30
CASSCF-NEVPT2	431.7	1.34	424.4	1.31
Experiment	418	0.63		

## 2. Excitation Wavelength Dependence of the Triplet State TREPR Spectra.

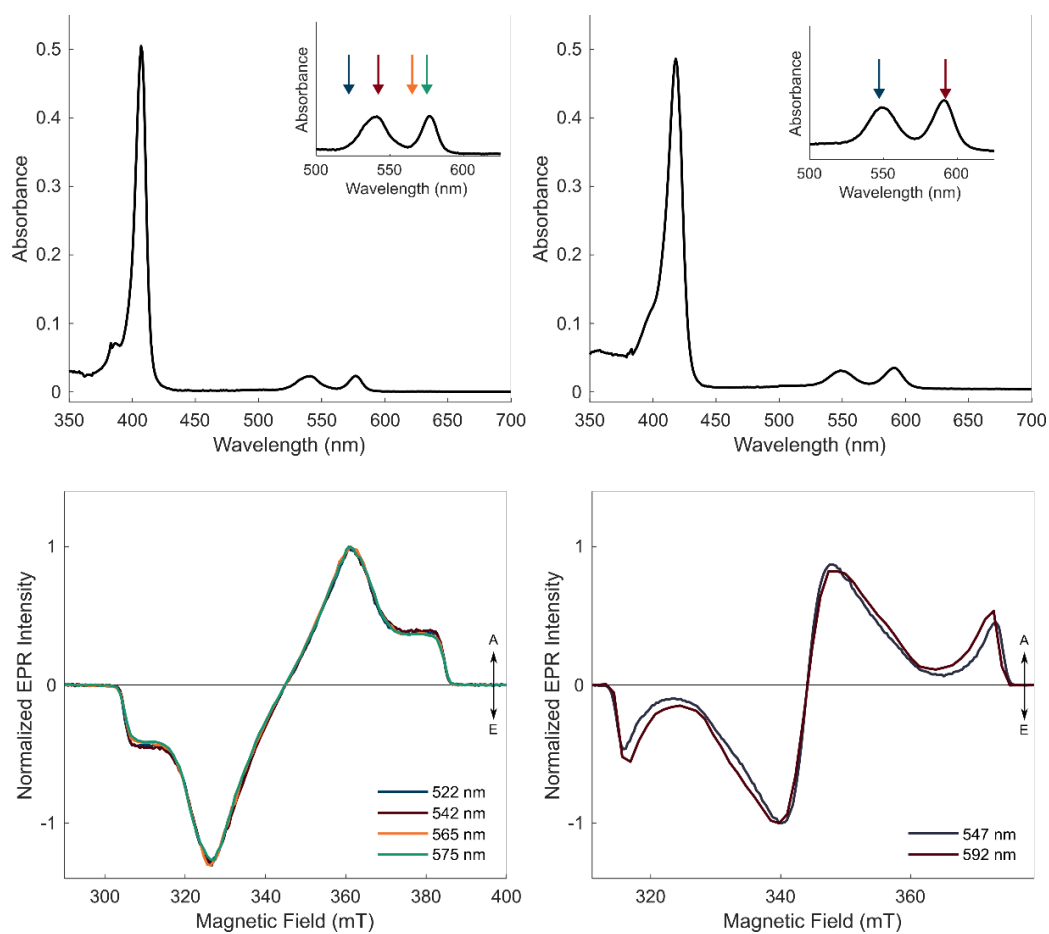


**Fig. S2.** Excitation wavelength dependence of the triplet state TREPR spectrum of AlPor-OH and PPor-OMe-PF<sub>6</sub> in 3:1 MeTHF:CH<sub>2</sub>Cl<sub>2</sub> at 80 K

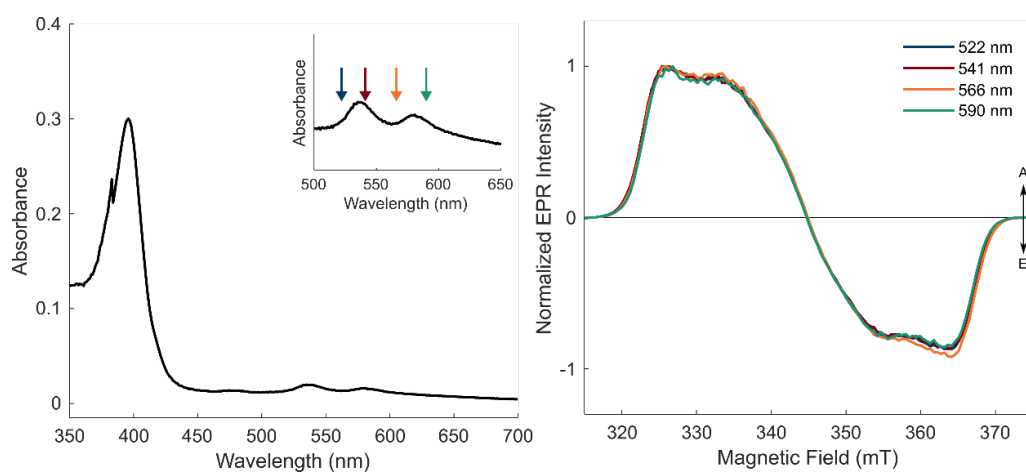


**Fig. S3.** Excitation wavelength dependence of the triplet state TREPR spectrum of AlPor-O-PPor-OMe-PF<sub>6</sub> in 3:1 MeTHF:CH<sub>2</sub>Cl<sub>2</sub> at 80 K.

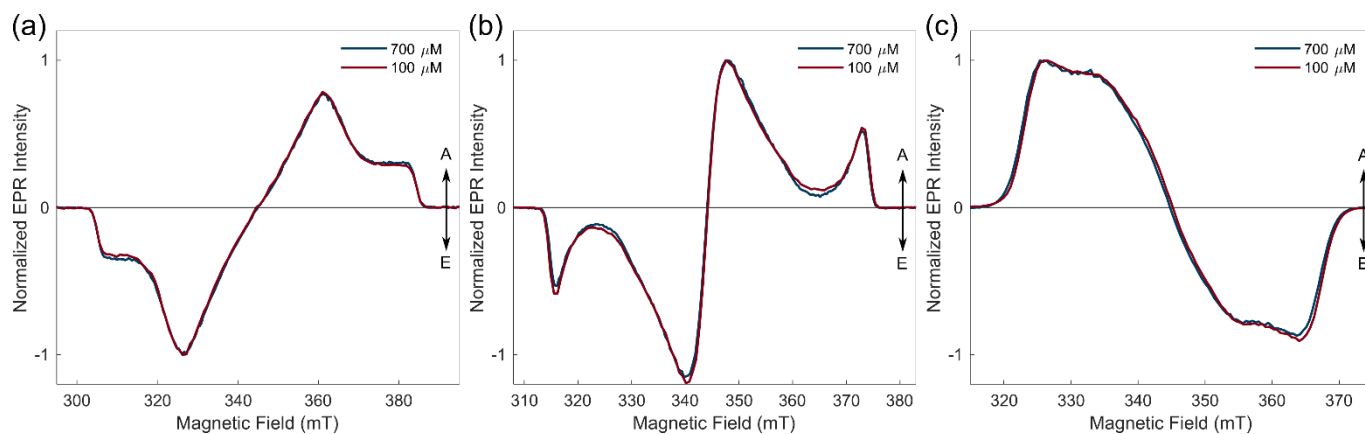


**Fig. S4.** Concentration dependence of the X-band triplet state TREPR spectrum of (a) AlPor-OH (b) PPor-OMe-PF<sub>6</sub> and (c) AlPor-O-PPor-PF<sub>6</sub> in 3:1 MeTHF:CH<sub>2</sub>Cl<sub>2</sub> at 80 K.

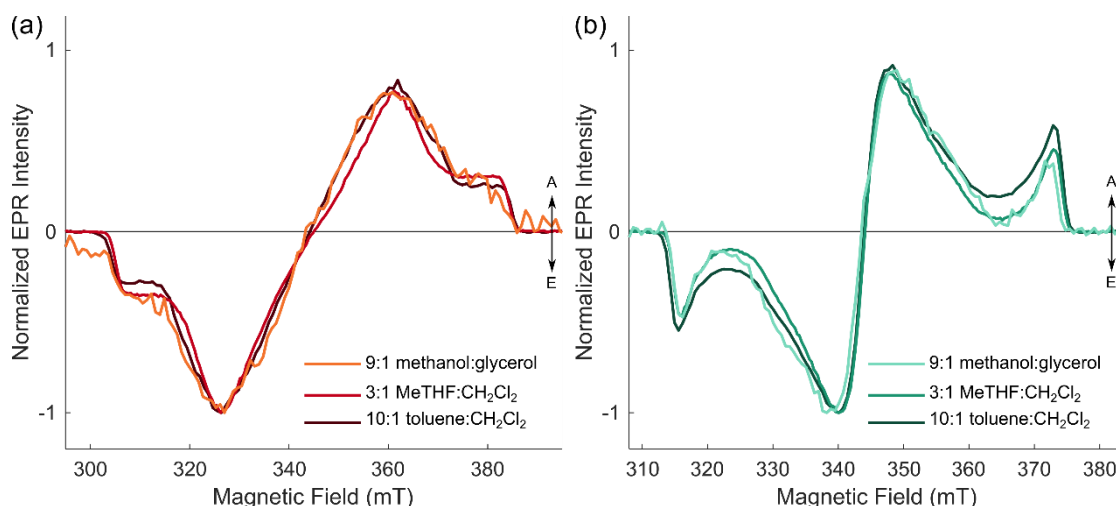


**Fig. S5** Solvent dependence of the transient EPR spectra of (a) AlPor-OH and (b) PPor-OMe-PF<sub>6</sub> at 80 K. The spectra were extracted from the time/field dataset in a time window centred at  $\sim 1 \mu\text{s}$  after the laser flash ( $\lambda_{\text{ex}} = \sim 540 \text{ nm}$ ).

### 3. Experimental and Simulated Q-band Triplet State TREPR Spectra.

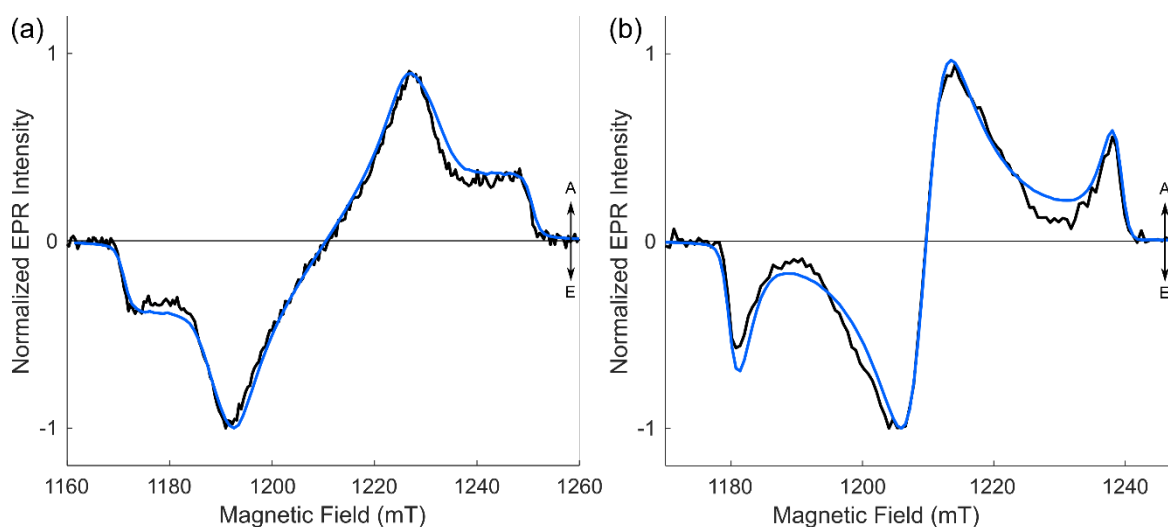


**Fig. S6** Experimental and simulated Q-band transient EPR spectra of (a) AlPor-OH and (b) PPor-OMe-PF<sub>6</sub> in 3:1 MeTHF:CH<sub>2</sub>Cl<sub>2</sub> at 80 K.

### 4. Magnetophotoselection

The spectra collected with different relative orientations of the polarization of the laser relative to the magnetic field have been simulated to obtain quantitative information on the relative orientation between the optical transition dipole moment and the principal axes of the ZFS tensor. In these simulations, the magnetophotoselection is included as the excitation probability for each orientation of the molecule relative to the laboratory axis system. This probability depends on the relative orientation between the transition dipole moment ( $\mu$ ) and the direction polarization of light<sup>1</sup>:

$$p(\alpha, \beta, \gamma) = \frac{(\hat{u}_\mu \cdot \hat{u}_E)^2}{N} \quad (1)$$

where  $\alpha$ ,  $\beta$  and  $\gamma$  are angles describing the relative orientation of the molecular frame of reference and the laboratory axis system.  $\hat{u}_\mu$  and  $\hat{u}_E$  are unit vectors parallel to the transition dipole moment and the electric field component of the light. The definitions of the angles and relationship between the axis systems is shown in Fig. S7 when the polarization of the light is perpendicular to the field.

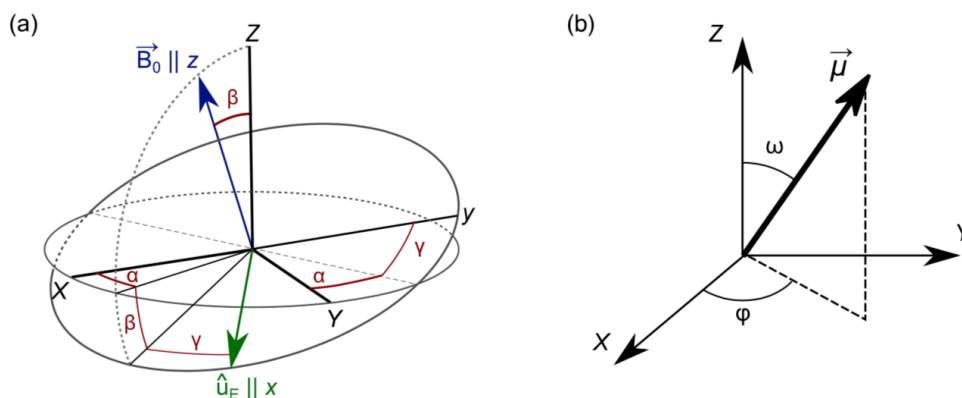


**Fig. S7** (a) Definition of the angles describing the relative orientation of laboratory frame ( $x, y, z$ ) and the ZFS frame ( $X, Y, Z$ ) with the electric field of the light perpendicular to the field. (b) Angles defining the orientation of the transition dipole moment relative to the ZFS axes.

The intensity of the EPR signal is given by<sup>2</sup>:

$$I_{ab}(B) = \sum_{\pm} \int_0^{\pi} \int_0^{2\pi} G\{B_{res}(\alpha, \beta) - B_0\} \cdot P_{\pm}(\alpha, \beta, B_0) \left[ \int_0^{2\pi} p_{\omega, \phi}^{par/perp}(\alpha, \beta, \gamma) d\gamma \right] \sin \beta d\alpha d\beta \quad (2)$$

where  $G\{B_{res}(\alpha, \beta) - B_0\}$  is a Gaussian lineshape function centred at the resonance field,  $P_{\pm}(\alpha, \beta, B_0)$  is the non-Boltzmann population difference between the two spin states in resonance and  $p_{\omega, \phi}^{par/perp}$  is the excitation probability with the electric field of the light parallel or perpendicular to the magnetic field  $B_0$ . Complete details of the distribution functions are given in Barbon et al<sup>1,2</sup>.

## 5. Calculated Triplet State Properties

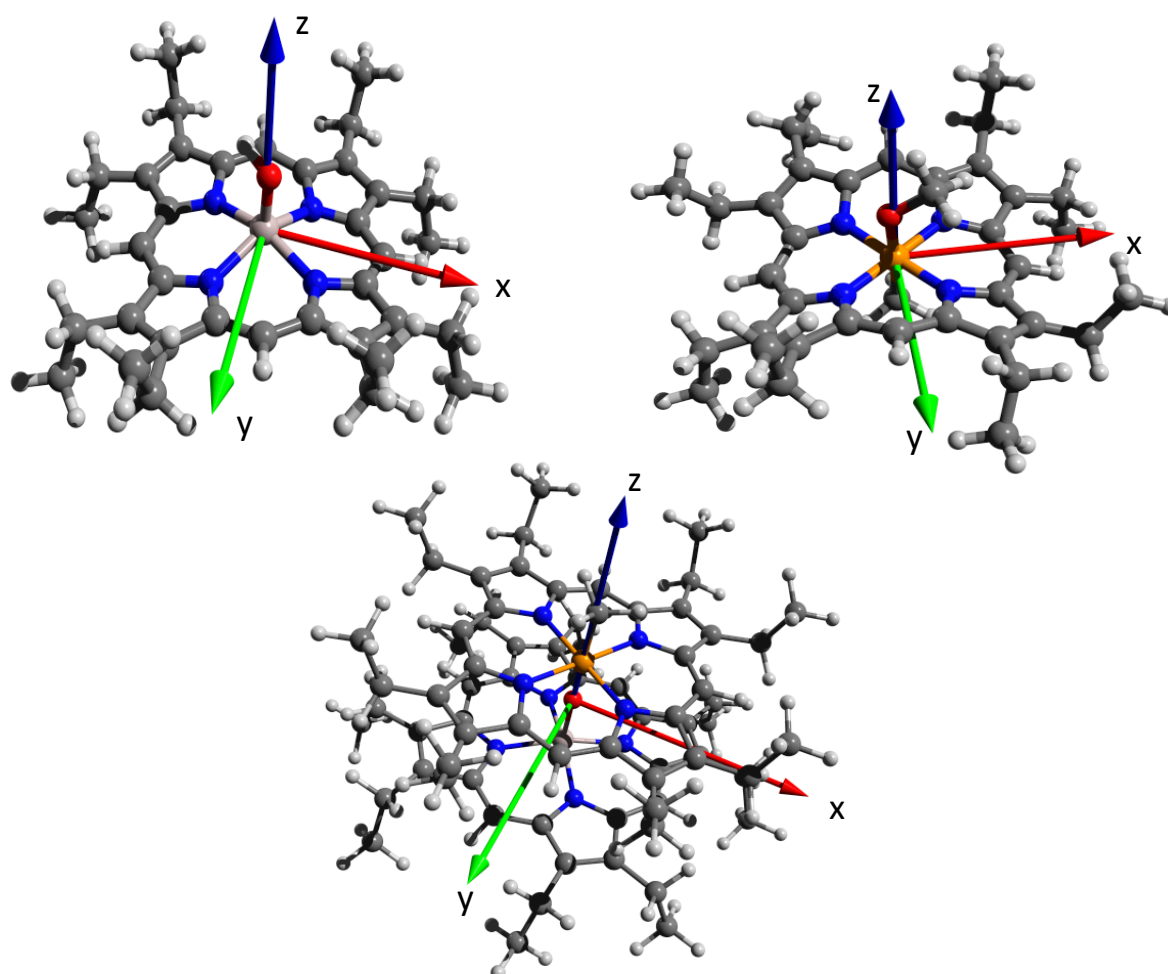


**Fig. S8** Orientation of the principal axes of the ZFS tensor in AlPor-OH, PPor-OMe<sup>+</sup> and AlPor-O-PPor<sup>+</sup> obtained from CASSCF-NEVPT2 calculations.

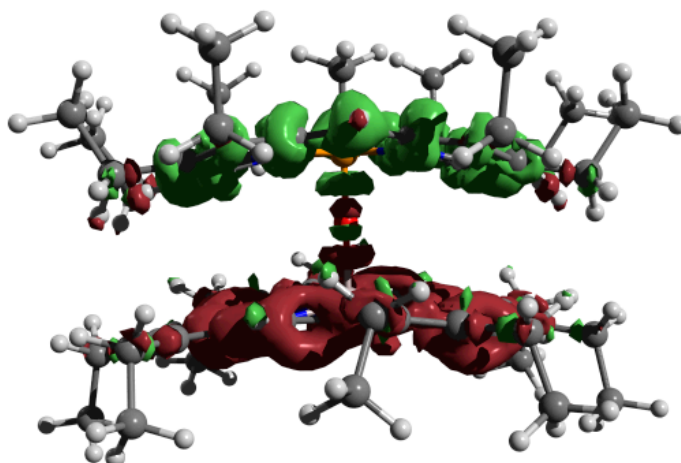


**Fig. S9** Triplet-minus-singlet electron density difference in AlPor-O-PPor<sup>+</sup> obtained from CASSCF calculations. The electron density difference was obtained by calculating the density in the lowest triplet state and the singlet ground state using the geometry optimized in the ground state. The density difference was obtained by subtracting cube files of the electron densities using Multiwfn<sup>3</sup>. The surface was plotted using Avogadro<sup>4</sup> with an iso value of 0.0005

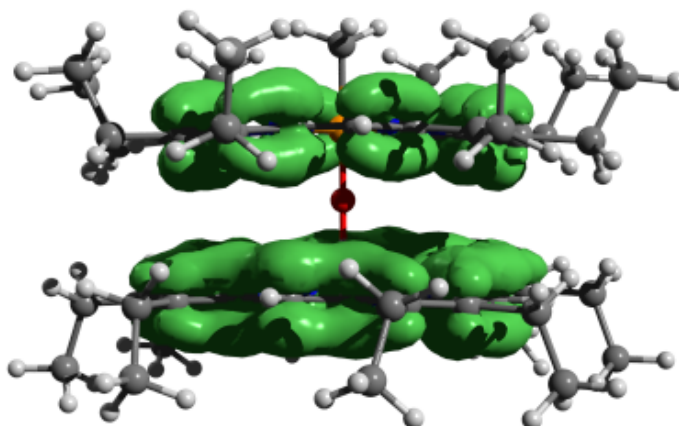


**Fig. S10** Triplet state spin density in AlPor-O-PPor<sup>+</sup> obtained from CASSCF-NEVPT2 calculations.

## References

- 1 A. Toffoletti, Z. Wang, J. Zhao, M. Tommasini and A. Barbon, Precise determination of the orientation of the transition dipole moment in a Bodipy derivative by analysis of the magnetophotoselection effect, *Phys. Chem. Chem. Phys.*, 2018, **20**, 20497–20503.
- 2 A. Barbon, M. G. Dal Farra, S. Ciuti, M. Albertini, L. Bolzonello, L. Orian and M. Di Valentin, Comprehensive investigation of the triplet state electronic structure of free-base 5, 10, 15, 20-tetrakis (4-sulfonatophenyl) porphyrin by a combined advanced EPR and theoretical approach, *J. Chem. Phys.*, 2020, **152**, 034201.
- 3 T. Lu and F. Chen, Multiwfn: a multifunctional wavefunction analyzer, *J. Comput. Chem.*, 2012, **33**, 580–592.
- 4 M. D. Hanwell, D. E. Curtis, D. C. Lonie, T. Vandermeersch, E. Zurek and G. R. Hutchison, Avogadro: an advanced semantic chemical editor, visualization, and analysis platform, *J. Cheminformatics*, 2012, **4**, 17.